

A novobiocin derivative, XN4, triggers ferroptosis in gastric cancer cells via the activation of NOX4

Rongrong Li^a, Bin Yin^b, Deyu Zeng^a and Zhenyang Liu^a

^aDepartment of Medical Oncology-Gastroenterology and Urology, Hunan Cancer Hospital, Affiliated Cancer Hospital of Xiangya School of Medicine, Central South University, Changsha, China; ^bDepartment of Gastric Pancreatic Surgery, Hunan Cancer Hospital, Affiliated Cancer Hospital of Xiangya School of Medicine, Central South University, Changsha, China

ABSTRACT

Context: A novobiocin derivative, XN4, has been shown to promote cell apoptosis in chronic myeloid leukaemia.

Objective: This study explores the mechanism by which XN4 promotes ferroptosis of gastric cancer (GC) cells.

Materials and methods: Human GC SGC-7901 and BGC-823 cells were treated with different XN4 concentrations (0, 0.1, 0.5, 1.0, 5.0, and 10.0 $\mu\text{mol/L}$) to evaluate effects of XN4. Additionally, cells were pre-treated for 24 h with si-NOX4, for 1 h with the iron chelator deferoxamine mesylate (DFO) or for 1 h with the lipid peroxidation inhibitor liproxstatin-1 before being treated with XN4 to analyse the mechanism of XN4.

Results: XN4 increased cell death (IC_{50} values of XN4 on SGC-7901 and BGC-823 cells: $1.592 \pm 0.14 \mu\text{mol/L}$ and $2.022 \pm 0.19 \mu\text{mol/L}$) and Fe^{2+} levels in SGC-7901 and BGC-823 cells. These effects of 2.0 $\mu\text{mol/L}$ XN4 were abolished by 100 $\mu\text{mol/L}$ DFO treatment. XN4 enhanced transferrin and transferrin receptor expression to induce Fe^{2+} accumulation. XN4 decreased mitochondrial membrane potentials in GC cells, similar to erastin. Additionally, XN4 increased MDA, hydrogen peroxide, and ROS levels, but diminished total glutathione levels. Liproxstatin-1 (200 nmol/L) nullified the effects of XN4 (2.0 $\mu\text{mol/L}$) on MDA levels and cell death. Moreover, GPX4 levels decreased, but NOX4 and ferroptosis-related protein PTGS2 levels increased in GC cells following XN4 treatment, which was nullified by NOX4 knockdown.

Discussion and conclusions: The pro-ferroptotic role of XN4 in GC might enable it to become a promising drug for GC treatment in the future despite the need for extensive research.

ARTICLE HISTORY

Received 7 January 2022

Revised 28 June 2022

Accepted 4 July 2022

KEYWORDS

Malondialdehyde; deferoxamine mesylate; erastin; liproxstatin-1; lipid peroxidation; mitochondrial damage

Introduction

Gastric cancer (GC) is the fifth most prevalent cancer worldwide, with the third highest mortality (Chen et al. 2016; Bray et al. 2018). In patients with advanced GC, metastasis is one of the key processes that negatively affect their prognosis (Zhao et al. 2021). Progress has been made in recent years in the systemic treatment of metastatic GC (Ooki and Yamaguchi 2021). However, the prognosis of patients with metastatic GC remains unfavourable with a 5-year overall survival rate of approximately 5%–20% (Wagner et al. 2017). Thus, novel therapeutic strategies for early GC are urgently needed to prevent this disease from further progressing to metastasis GC.

Cell death is strictly modulated by complex extracellular and intracellular signals and is essential for a variety of biological processes, such as homeostasis (Zhang et al. 2020). Cancer cells exhibit metabolic adaptation strategies to survive and facilitate tumour progression, including blocking apoptosis and non-apoptotic cell death pathways (Hanahan and Weinberg 2011; Pavlova and Thompson 2016). Unlike necrosis, apoptosis, and autophagy, ferroptosis features the accumulation of iron-dependent lipid peroxides (Cao and Dixon 2016; Stockwell et al. 2017). A recent

study has shown that ferroptosis is associated with multiple pathological processes, including neurodegeneration and acute renal failure (Fearnhead et al. 2017). Additionally, there is mounting evidence of the essential role of ferroptosis in mediating tumour progression in some types of cancer, including GC. However, the detailed molecular mechanism remains poorly understood (Jiang et al. 2015; Zhang et al. 2018; Sun et al. 2020). Therefore, regulation of cancer cell ferroptosis is emerging as an effective approach for cancer treatment.

Novobiocin (Nov) is a type of coumarin antibiotic, which, along with its synthetic derivatives, displays high efficacy in anti-proliferative assays against various cancer cell lines (Lettni et al. 2017). Several reports have demonstrated that Nov acts as a potential anticancer agent by leading to cell death in human cancer cells (Dlugosz and Janecka 2017; Le Bras et al. 2007). In order to explore more efficacious anticancer agents, we synthesised a series of Nov derivatives and found XN4 to be one of the most active agents. In Imatinib-sensitive and -resistant chronic myeloid leukaemia cells, XN4 has been reported to generate reactive oxygen species (ROS), resulting in DNA damage and cell apoptosis (Wu et al. 2015). Although no studies have reported the relationship between XN4 and ferroptosis of cancer

cells, increasing evidence suggests that Nov may induce apoptosis and that ferroptosis occurs simultaneously with apoptosis and autophagy (Wu et al. 2008; Hou et al. 2016; Hong et al. 2017). Therefore, XN4 might have potential as a cancer treatment. In this study, we explore the possible effect of XN4 on the ferroptosis of GC cells and determine the potential role of nicotinamide adenine dinucleotide phosphate oxidase 4 (NOX4) in this process.

Materials and methods

Cell culture

Human GC cell lines (SGC-7901 and BGC-823) and human normal gastric mucosal epithelial cell line (GES-1) (all from American Type Culture Collection, Manassas, VA, USA) were cultured in Dulbecco's modified Eagle's medium (Gibco, Grand Island, NY, USA) supplemented with 10% foetal bovine serum and 1% penicillin/streptomycin in a 5% CO₂ atmosphere at 37 °C.

XN4 treatment

XN4 was synthesised and purified by our group and then dissolved in dimethyl sulfoxide (DMSO). SGC-7901 and BGC-823 cells were separately treated with different concentrations of XN4 (0, 0.1, 0.5, 1.0, 5.0, and 10.0 µmol/L) for 48 h and then used for subsequent experiments.

Cell transfection

The small interfering RNA (siRNA/si) of NOX4 (si-NOX4, 2 µg, F: 5'-UGUUUAACCCCUUCGUUGGCG-3', R: 5'-CCAACGAAGGGGUUAAACACC-3') and its negative control (si-NC, 2 µg) were synthesised by GenePharma (Shanghai, China). All transfections were carried out as per the lipofectamine 2000 kit (Invitrogen, Carlsbad, CA, USA) manual. Following 24 h transfection with si-NOX4 or si-NC, SGC-7901 and BGC-823 cells were used in the following studies.

Inhibitor treatment

To detect ferroptosis, SGC-7901 and BGC-823 cells were separately treated with either 100 µmol/L iron chelator deferoxamine mesylate (DFO; S5742) or 200 nmol/L liproxstatin-1 (the lipid peroxidation inhibitor, S7699, Selleck, Houston, TX, USA) for 1 h before XN4 treatment.

3-(4, 5-Dimethylthiazol-2-yl)-2, 5-diphenyltetrazolium bromide (MTT) assay

SGC-7901 and BGC-823 cells treated with si-NOX4, si-NC, XN4, or ferroptosis inhibitors (DFO or liproxstatin-1) were trypsinized and seeded into 96-well plates (1,000 cells/well) in a humid atmosphere containing 5% CO₂ at 37 °C for 24 h. Three duplicates were processed for each condition. After the supernatant was discarded, cells were washed with a culture medium three times before a 4 h incubation with a serum-free medium (100 µL/well) in an incubator. Thereafter, the supernatant was carefully discarded and 10 µL MTT dissolved in DMSO was added (at a final concentration of 5 mg/mL; Sigma-Aldrich, Merck KGaA, Darmstadt, Germany). The optical density (OD)

value at 570 nm was recorded. The absorbance was proportional to the number of living cells.

Lactate dehydrogenase (LDH) assay

SGC-7901 and BGC-823 cells were treated with si-NOX4, si-NC, XN4, or ferroptosis inhibitors and then seeded into a 96-well plate, followed by 5 min centrifugation at 1,500 rpm. The supernatant (120 µL) was added to another 96-well plate to measure the OD value of LDH released by the cells. An LDH Assay Kit (Beyotime, Shanghai, China) was used to detect the LDH content of the cell cultures. The OD value was recorded at 490 nm and all operations were carried out strictly following the kit protocols. The absorbance of wells containing only fresh culture medium was used to determine the background absorbance. Control cells were permeabilized with 1% Triton X-100 for 60 min to obtain the cell lysates, and the maximum absorbance was recorded. LDH release = (sample absorbance - background absorbance)/(maximum absorbance - background absorbance) × standard concentration. The cell death rate was directly proportional to the LDH release rate.

Iron assay

The intracellular ferrous iron (Fe²⁺) level was assessed using the iron assay kit (ab83366, Abcam, Cambridge, UK) according to the manufacturer's manuals. Briefly, samples or standards were homogenised in iron assay buffer at room temperature for 30 min. Then, the iron probe was incubated with the samples for 60 min at room temperature. Finally, the OD value was measured at 593 nm.

Malondialdehyde (MDA) assessment

The relative concentration of the lipid peroxidation end product MDA in cell lysates was determined using a lipid peroxidation (MDA) assay kit (ab118970, Abcam). Specifically, the MDA in the sample was reacted with thiobarbituric acid (TBA) to generate an MDA-TBA adduct that was then quantified colorimetrically (OD_{532 nm}).

Detection of hydrogen peroxide

A hydrogen peroxide detection kit (S0038, Beyotime) was employed to measure the hydrogen peroxide content of the cells. Cells were centrifuged with the supernatant removed. Then, 10⁶ cells were lysed with 150 µL hydrogen peroxide lysis buffer and centrifuged at 4 °C and 12,000 × g for 3–5 min. The supernatant was harvested for further use. The concentration of hydrogen peroxide was detected using an ultraviolet spectrophotometer according to the standard curve.

Detection of total glutathione (TGSH) and mitochondrial membrane potentials

The concentration of TGSH in cells was determined using a TGSH kit (S0052, Beyotime) as per the manufacturer's protocols. JC-1 staining solution was added to cells, followed by several rounds of gentle trituration and incubation for 20 min in an incubator. Cells were then centrifuged and the supernatant was discarded before the addition of 1 mL JC-1 staining solution to

re-suspend the cells. Next, cells were centrifuged and the supernatant was discarded, and this process was repeated. The cells in the tubes were resuspended by the addition of 200 μ L JC-1 staining solution. The fluorescence intensity was measured using a flow cytometer within 30 min.

Intracellular ROS level measurement

The intracellular production of ROS was assessed using the 5-(and-6-)chloromethyl-2',7'-dichlorodihydro-fluorescein diacetate (CMH2DCF-DA) probe (Thermo Fisher Scientific, Waltham, MA, USA). Briefly, the cell culture medium was removed and the cells were washed in pre-warmed phosphate-buffered saline (PBS). The cells were then incubated for 30 min in PBS containing 10 μ M of the probe. A flow cytometer was used to detect the fluorescence intensity of oxidised 2',7'-dichlorofluorescein (DCF).

Quantitative real-time polymerase chain reaction (qRT-PCR)

Total RNAs were extracted using TRIzol reagents (Invitrogen) and reverse transcription was performed using the reverse transcription kit (TaKaRa, Tokyo, Japan) following the manufacturers' protocols. Gene expression was detected using the LightCycler 480 Real-Time PCR System (Roche Diagnostics, Indianapolis, IN, USA). The reaction condition was set in the light of the manuals of the fluorescent quantitative RT-PCR kit (SYBR Green Mix, Roche Diagnostics), including pre-denaturation at 95 $^{\circ}$ C for 10 s and 45 cycles of denaturation at 95 $^{\circ}$ C for 5 s, annealing at 60 $^{\circ}$ C for 10 s, and extension at 72 $^{\circ}$ C for 10 s, followed by a final extension at 72 $^{\circ}$ C for 5 min. Each PCR was repeated thrice. Glyceraldehyde 3-phosphate dehydrogenase (GAPDH) functioned as an internal reference and data were analysed using the $2^{-\Delta\Delta C_t}$ method: $\Delta\Delta C_t = [C_{t_{\text{target gene}}} - C_{t_{\text{reference gene}}}]_{\text{experimental group}} - [C_{t_{\text{target gene}}} - C_{t_{\text{reference gene}}}]_{\text{control group}}$. The amplified primers are depicted in Table 1.

Western blot

Cells were lysed in radio-immunoprecipitation assay buffer (Beyotime) to obtain protein samples. The total protein concentration was measured using a bicinchoninic acid assay kit (Beyotime). Then, proteins were denatured in boiling water for 3 min and electrophoresis was initially conducted at 80 V for 30 min and then at 120 V for 1–2 h. The proteins were then transferred onto the membrane in an ice bath at 300 mA for 60 min. Afterwards, the membrane was rinsed in washing buffer for 1–2 min and then blocked at room temperature for 60 min or 4 $^{\circ}$ C overnight to avoid unspecific responses. The membrane was incubated with primary antibodies against glutathione peroxidase

(GPX4; ab125066, 1:1,000), transferrin (TF; ab277635, 1:1,000), transferrin receptor (TFR; ab269513, 1:5,000), ferritin H (FTH; ab75972, 1:1,000), ferritin L (FTL; ab109373, 1:10,000), ferroportin (FPN; ab239511, 1:1,000), prostaglandin-endoperoxide synthase 2 (PTGS2; ab15191, 1:1,000), NOX4 (ab133303, 1:1,000), or GAPDH (ab181602, 1:10,000) (Abcam) on a shaker for 1 h at room temperature, followed by washing for 3×10 min. Subsequently, the membrane was incubated with secondary antibodies for 1 h at room temperature before washing for 3×10 min. The proteins on the membrane were detected on a chemiluminescence imaging system (Gel Doc XR, Bio-Rad, Hercules, CA, USA) subsequent to the addition of developing solutions.

Statistical analysis

Data were analysed using GraphPad Prism 7 Software (GraphPad Software Inc., San Diego, CA, USA). Continuous data were presented as mean \pm standard deviation. Two groups were compared using the independent-samples Student's *t*-test, and comparisons among multiple groups were evaluated using the one-way analysis of variance (ANOVA) test, followed by Dunnett's multiple comparisons test or Tukey's multiple comparisons test. $p < 0.05$ was regarded as a statistically significant difference.

Results

XN4 induced death in GC cells

The molecular structure in Figure 1A is the synthesised XN4 (3-chlorine-2 ether phenol-1,4-naphthoquinone; its molecular weight was 490 kD) with over 95% purity. SGC-7901 and BGC-823 cells were treated with different concentrations of XN4. The MTT assay found that different concentrations of XN4 significantly inhibited the viability of SGC-7901 and BGC-823 cells ($p < 0.05$) (Figure 1B and C); the IC_{50} of XN4 on SGC-7901 cells was 1.592 ± 0.14 μ mol/L and the IC_{50} of XN4 on BGC-823 cells was 2.022 ± 0.19 μ mol/L. Cell death was assessed using the LDH release assay and the results indicated that XN4 induced SGC-7901 and BGC-823 cell death ($p < 0.05$) (Figure 1D and E). Treatment with XN4 had almost no influence on the cell viability and death of GES-1 cells (Figure 1F and G). These results indicated that XN4 induced GC cell death.

Iron regulated XN4-induced GC cell death

To determine whether XN4 elicited ferroptosis in GC cells, the level of Fe^{2+} was investigated in XN4-treated GC cells. The level of intracellular Fe^{2+} increased in SGC-7901 and BGC-823 cells following XN4 treatment ($p < 0.05$) (Figure 2A and B). Next, GC cells were treated with DFO (100 μ mol/L) for 1 h, followed by 2.0 μ mol/L XN4 treatment. DFO significantly inhibited the XN4-induced increase in Fe^{2+} levels in SGC-7901 and BGC-823 cells ($p < 0.05$) (Figure 2C and D). The MTT results showed that the significant inhibitory effect of XN4 on SGC-7901 and BGC-823 cell viability was reversed by DFO treatment ($p < 0.05$) (Figure 2E and F). The LDH release assay demonstrated that DFO had an obvious inhibitory effect on XN4-induced GC cell death ($p < 0.05$) (Figure 2G and H). These results indicated that XN4 triggered ferroptosis in SGC-7901 and BGC-823 cells since the apoptosis of GC cells induced by XN4 was associated with increases in Fe^{2+} expression in cells.

Table 1. Primer sequences.

Name of primer	Sequences
GPX4-F	TTCCCGTGTAAACAGTTCGG
GPX4-R	GTGGAGAGACGGGTGCCAAA
PTGS2-F	GTTCCACCCGAGTACAGAA
PTGS2-R	AGGGCTTCAGCATAAAGCGT
NOX4-F	CAGTCITTGACCCTCGGTCC
NOX4-R	TTTAACCCCTTCGTTGGCGA
GAPDH-F	AATGGGCAGCCGTAGGAAA
GAPDH-R	GCGCCAATACGACCAATC

Note: F, forward; R, reverse.

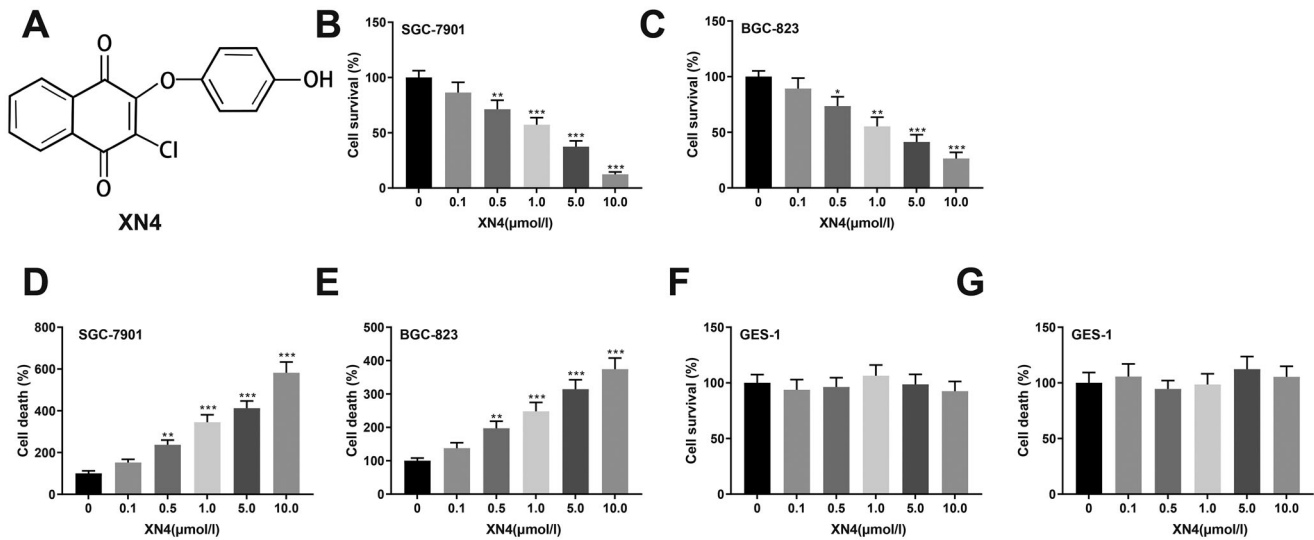


Figure 1. XN4 induced gastric cancer (GC) cell death. The molecular structure of XN4 (A). After SGC-7901 and BGC-823 cells were treated with different concentrations of XN4, cell viability was tested by MTT assay (B, C), and cell death was probed by the lactate dehydrogenase (LDH) release assay (D, E). Cell viability of GES-1 cells treated with various concentrations of XN4 was detected by MTT assay (F). The cell death of GES-1 cells treated with various concentrations of XN4 was measured by the LDH release assay (G). * $p < 0.05$, ** $p < 0.01$, *** $p < 0.001$ vs. the XN4 (0 μmol/L) group.

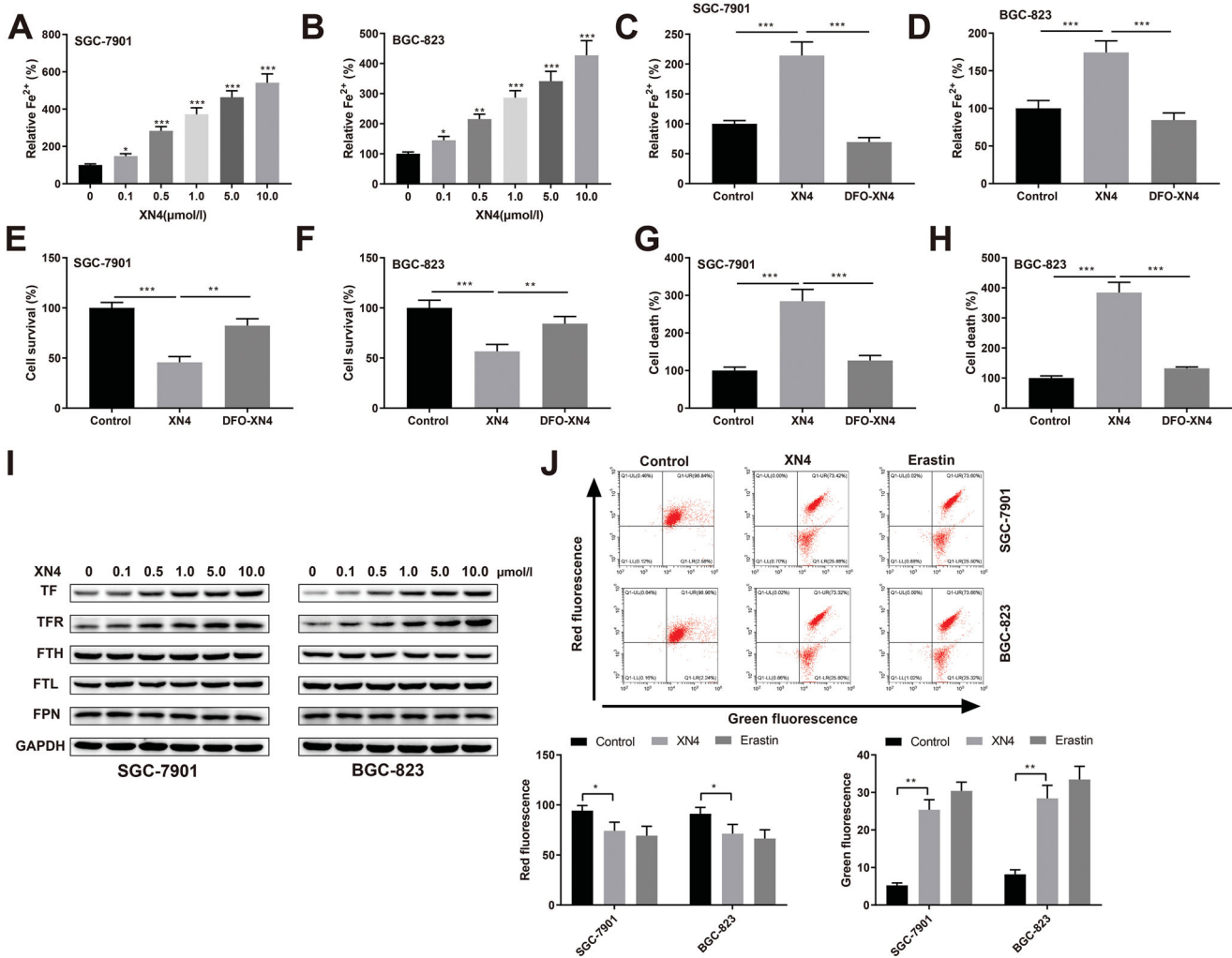


Figure 2. Iron orchestrated XN4-induced gastric cancer (GC) cell death. The levels of intracellular Fe²⁺ were tested by an iron assay kit after SGC-7901 and BGC-823 cells were separately treated with different concentrations of XN4 (A, B). After SGC-7901 and BGC-823 cells were treated with deferoxamine mesylate (DFO) or/and XN4, the levels of Fe²⁺ were monitored by the iron assay kit (C, D), cell viability was probed by MTT assay (E, F), and cell death was determined by the lactate dehydrogenase (LDH) release assay (G, H). Western blot was used to detect the expression of transferrin (TF), transferrin receptor (TFR), ferritin H (FTH), ferritin L (FTL), and ferroportin (FPN) in XN4-treated GC cells (I). The mitochondrial membrane potential of XN4-treated GC cells was measured by flow cytometry (J). * $p < 0.05$, ** $p < 0.01$, *** $p < 0.001$ vs. the XN4 (0 μmol/L) group, the control group, or the XN4 group.

To explore the reason for XN4-induced elevation in Fe^{2+} expression in GC cells, a western blot was implemented to detect TF, TFR, FTH, FTL, and FPN expression. The western blot revealed that TF and TFR expression increased after XN4 treatment, whereas no change in FTH, FTL, and FPN expression was observed (Figure 2I), indicating that XN4 facilitated Fe accumulation in GC cells by upregulating TF and TFR, instead of suppressing FTH, FTL, and FPN expression. Erastin is a strong trigger of ferroptosis (Dixon et al. 2012), so we used erastin as a positive control in this study. As a feature of ferroptosis, mitochondrial damage was detected using the JC-1 probe. Flow cytometry revealed decreased red fluorescence and elevated green fluorescence in XN4-treated SGC-7901 and BGC-823 cells, which was consistent with the observations in erastin-treated cells (Figure 2J).

XN4 induced lipid peroxidation in GC cells

A previous study revealed that lipid peroxidation is an important signalling event that triggers ferroptosis (Hu et al. 2021). To investigate the changes in lipid peroxidation during XN4-induced

ferroptosis, the lipid peroxidation end product MDA was measured in GC cells after XN4 treatment. The results revealed that MDA levels were elevated in GC cells following XN4 treatment ($p < 0.05$) (Figure 3A and B). Next, GC cells were treated with the lipid peroxidation inhibitor liproxstatin-1 (200 nmol/L) for 1 h, followed by 2.0 $\mu\text{mol/L}$ XN4 treatment. The data showed that liproxstatin-1 effectively suppressed the upregulation of MDA in SGC-7901 and BGC-823 cells induced by XN4 ($p < 0.05$) (Figure 3C and D). Moreover, the MTT assay revealed that XN4 substantially reduced SGC-7901 and BGC-823 cell viability, but this effect was abolished by liproxstatin-1 treatment ($p < 0.05$) (Figure 3E and F). The LDH release assay demonstrated that liproxstatin-1 clearly repressed the GC cell death induced by XN4 ($p < 0.05$) (Figure 3G and H). Meanwhile, the expression of hydrogen peroxide increased ($p < 0.05$) (Figure 3I and J) and the GSH level decreased ($p < 0.05$) (Figure 3K and L) in cells treated with XN4. XN4 treatment elevated intracellular ROS levels ($p < 0.05$) (Figure 3M and N). These data indicated that lipid peroxidation was involved in the GC cell death caused by XN4.

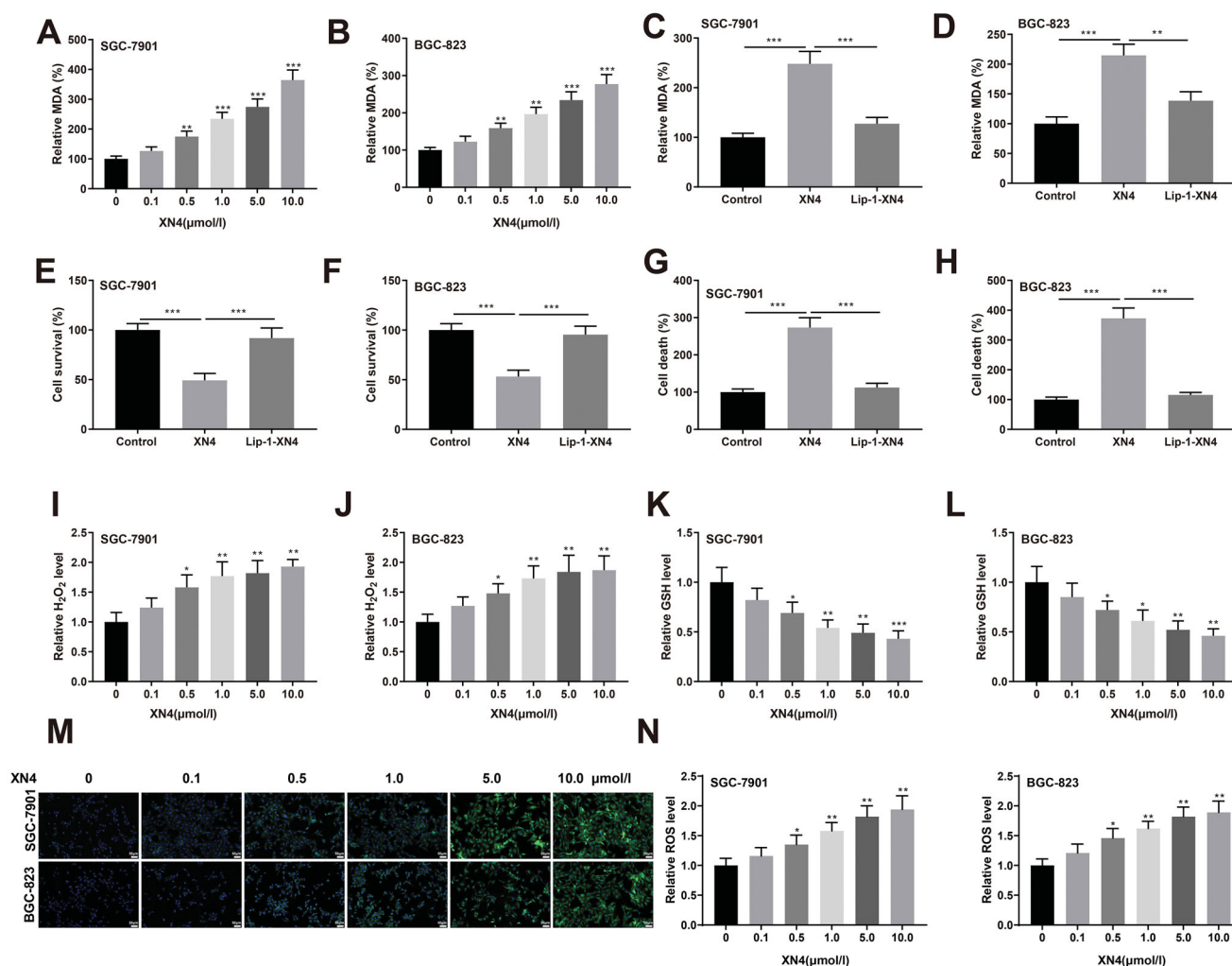


Figure 3. XN4 promoted lipid peroxidation in gastric cancer (GC) cells. The levels of malondialdehyde (MDA) were assayed by a lipid peroxidation (MDA) assay kit after SGC-7901 and BGC-823 cells were separately treated with different concentrations of XN4 (A, B). Following treatment of SGC-7901 and BGC-823 cells with liproxstatin-1 or/and XN4, the levels of MDA were measured by the lipid peroxidation (MDA) assay kit (C, D); cell viability was evaluated by MTT assay (E, F), and cell death was observed by the lactate dehydrogenase (LDH) release assay (G, H). The levels of hydrogen peroxide (I, J) and GSH (K, L) in XN4-treated SGC-7901 and BGC-823 cells were assessed using corresponding kits. The level of ROS in XN4-treated SGC-7901 and BGC-823 cells was measured using the flow cytometer (M, N, $\times 200$). * $p < 0.05$, ** $p < 0.01$, *** $p < 0.001$ vs. the XN4 (0 $\mu\text{mol/L}$) group, the control group, or the XN4 group.

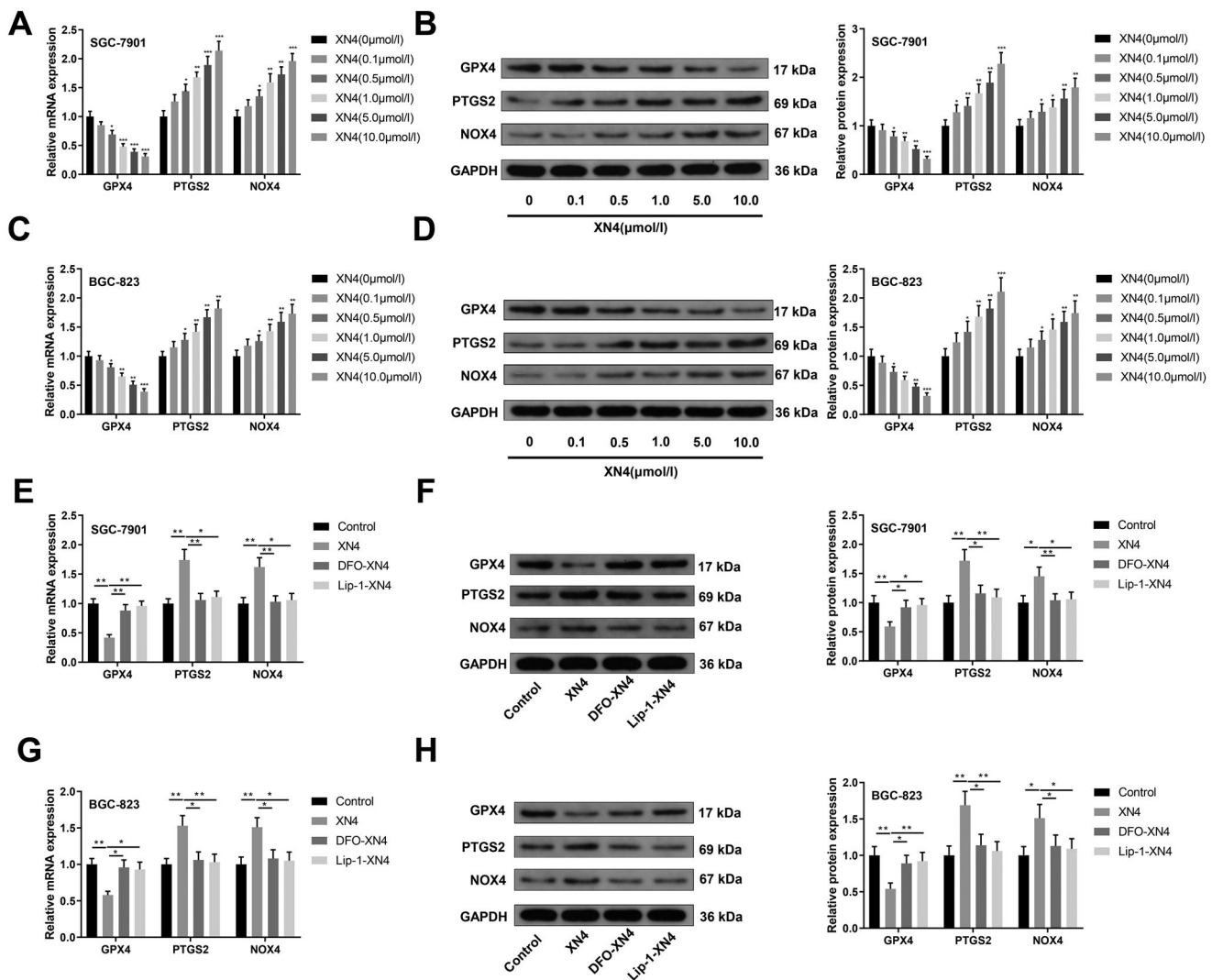


Figure 4. NOX4 was highly expressed in XN4-induced gastric cancer (GC) cells. After SGC-7901 (A, B) and BGC-823 (C, D) cells were treated with different concentrations of XN4, quantitative real-time polymerase chain reaction (qRT-PCR) and western blot were applied to determine the levels of ferroptosis-related proteins (GPX4 and PTGS2) and NOX4. After SGC-7901 (E, F) and BGC-823 (G, H) cells were treated with XN4 alone or with XN4 and deferoxamine mesylate (DFO)/liproxstatin-1, the expression of ferroptosis-related proteins and NOX4 were probed by qRT-PCR and western blot. * $p < 0.05$, ** $p < 0.01$, *** $p < 0.001$ vs. the XN4 (0 μmol/L) group, the control group, or the XN4 group.

NOX4 was upregulated in XN4-treated GC cells

GPX4 can protect against lipid peroxidation. To explore the mechanism by which XN4 induces ferroptosis, the levels of ferroptosis-related proteins (GPX4 and PTGS2) (Zhang et al. 2021) during the GC cell death induced by XN4 were measured using qRT-PCR for quantitative analysis and western blot for semi-quantitative analysis. As depicted in Figure 4A–D, GPX4 levels were diminished while PTGS2 levels were augmented in GC cells following XN4 treatment. In addition, the results revealed that NOX4 expression was elevated after XN4 treatment ($p < 0.05$). In astrocytes, NOX4 promotes ferroptosis via oxidative stress-induced lipid peroxidation (Park et al. 2021). In this study, DFO and liproxstatin-1 dampened the XN4-induced changes in the levels of ferroptosis-related proteins and NOX4 ($p < 0.05$) (Figure 4E–H). These results indicated that the effects of XN4 on ferroptosis-related proteins in GC cells were reversed by DFO and liproxstatin-1 treatments and that NOX4 was implicated in XN4-induced ferroptosis of GC cells.

XN4 promoted ferroptosis by upregulating NOX4

To further investigate whether NOX4 is involved in XN4-induced ferroptosis, SGC-7901 and BGC-823 cells were transfected with si-NOX4 and then treated with XN4. qRT-PCR for quantitative analysis and western blot for semi-quantitative analysis revealed that NOX4 expression was markedly decreased in the si-NOX4 group compared with the si-NC group ($p < 0.05$) (Figure 5A and B). The MTT assay showed that the inhibition of SGC-7901 and BGC-823 cell viability by XN4 was reduced by NOX4 knockdown ($p < 0.05$) (Figure 5C). The LDH release assay demonstrated that si-NOX4 significantly diminished XN4-triggered GC cell death ($p < 0.05$) (Figure 5D). Furthermore, si-NOX4 (2.0 μg) obviously inhibited the increases in MDA ($p < 0.05$) (Figure 5E), hydrogen peroxide ($p < 0.05$) (Figure 5F), and ROS ($p < 0.05$) (Figure 5G) levels in GC cells treated with XN4. The collective results indicated that NOX4 participated in the XN4-induced lipid peroxidation and ferroptosis in GC cells.

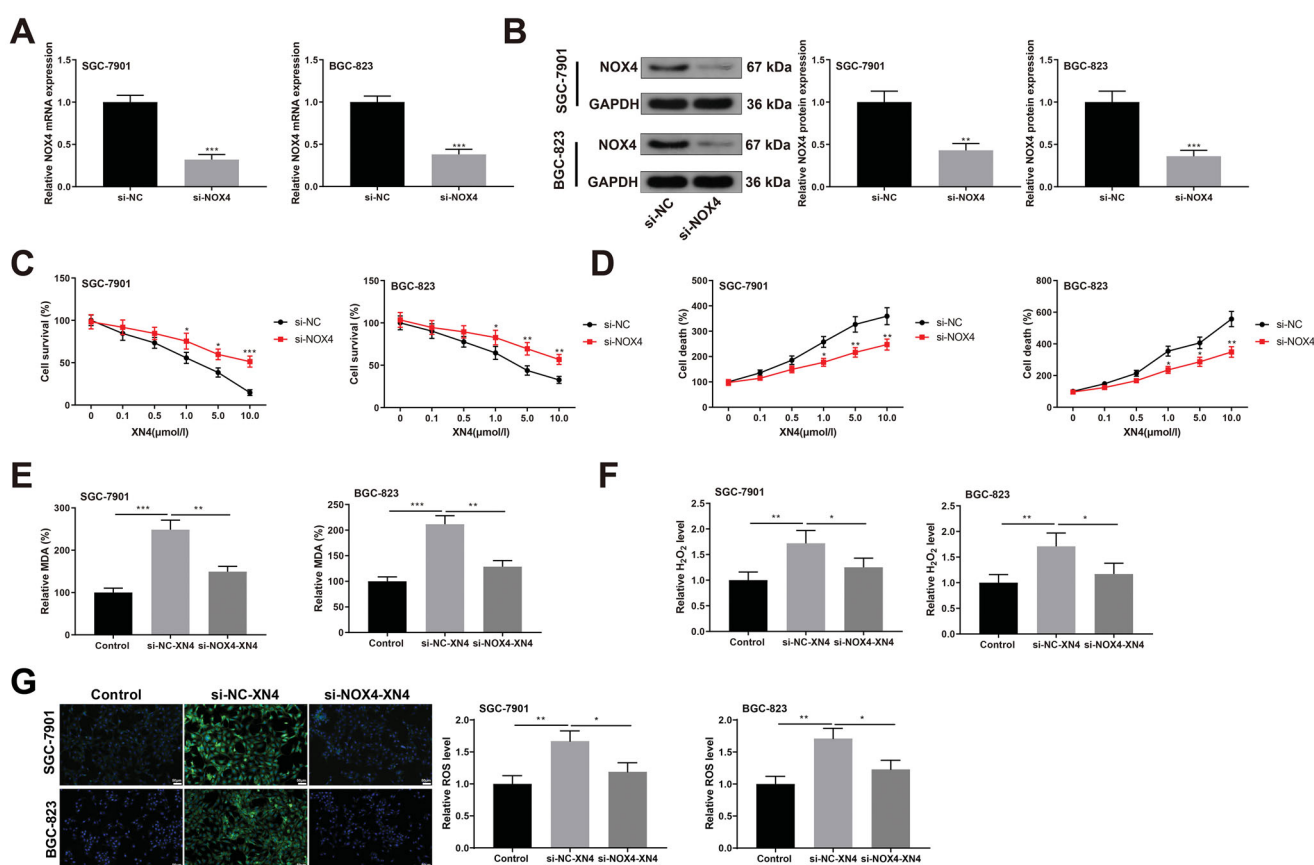


Figure 5. XN4 accelerated GC cells ferroptosis via NOX4 activation. After SGC-7901 and BGC-823 cells were transfected with si-NOX4 or si-NC, the levels of NOX4 were determined by quantitative real-time polymerase chain reaction (qRT-PCR) (A) for quantitative analysis and western blot (B) for semiquantitative analysis. After SGC-7901 and BGC-823 cells were transfected with si-NOX4 or si-NC and treated with XN4, cell viability was determined by MTT assay (C) and cell death was probed by the lactate dehydrogenase (LDH) release assay (D). The levels of malondialdehyde (MDA) (E) and hydrogen peroxide (F) in SGC-7901 and BGC-823 cells were measured after cell transfection and XN4 treatment. ROS levels in SGC-7901 and BGC-823 cells were assessed after cell transfection and XN4 treatment (G, $\times 200$). * $p < 0.05$, ** $p < 0.01$, *** $p < 0.001$ vs. si-NC group, or the control group.

Discussion

In this study, we demonstrated for the first time that XN4-induced ferroptosis of GC cells involved the activation of NOX4. In the current study, MTT and LDH release assays showed that XN4 treatment at various concentrations inhibited the viability of GC cells and obviously induced GC cell death. Ferroptosis has been established as a cell death pathway. Besides cancer, ferroptosis has a crucial role in many other pathophysiological processes and diseases (Friedmann Angeli et al. 2014; Linkermann et al. 2014; Skouta et al. 2014; Gao et al. 2015). A previous study has identified ferroptosis in GC progression (Hao et al. 2017), which indicated that ferroptosis might be a suitable target for GC treatment. In this regard, we investigated the effect of XN4 on the levels of Fe^{2+} to decipher whether XN4 potentiated ferroptosis in GC cells. We found that intracellular Fe^{2+} levels were increased in GC cells following XN4 treatment. When GC cells were treated with DFO and XN4, DFO strikingly suppressed the increase in Fe^{2+} levels induced by XN4 in GC cells. Additionally, the results of the MTT and LDH release assays demonstrated that XN4 decreased GC cell viability and facilitated cell death, and these effects were reversed by DFO treatment. These data revealed that XN4 triggered ferroptosis in GC cells. Ferroptosis-induced cell death can be reversed by iron chelators and lipid peroxidation inhibitors (Dixon et al. 2012; Yang et al. 2014). Ferrous iron-induced lipid peroxidation is regarded as a crucial

step for ferroptotic cell death (Dixon et al. 2012). Here, our study revealed that the lipid peroxidation end product MDA was upregulated in GC cells following XN4 treatment. Besides, we found that the lipid peroxidation inhibitor liproxstatin-1 effectively suppressed MDA production in GC cells treated with XN4. Moreover, our results showed that XN4 substantially reduced GC cell viability and induced cell death, but these effects were nullified by liproxstatin-1 treatment. Taken together, these data illustrated that XN4 induced an abnormal increase in intracellular Fe^{2+} and lipid peroxidation during the process of GC cell death. The iron chelator DFO and the lipid peroxidation inhibitor liproxstatin-1 inhibited XN4-induced death in GC cells. Thus, these data provide evidence that XN4 stimulates ferroptosis in GC cells.

Next, the probable mechanism by which XN4 stimulated ferroptosis was explored. NOX4, a NOX isoform frequently expressed in tumour cells, has been reported to interfere with cell proliferation, apoptosis, and cell cycle progressions in cancer cells, such as glioma, non-small cell lung cancer, and melanoma (Shono et al. 2008; Li et al. 2015; Tang et al. 2018). Furthermore, a previous study has confirmed that NOX4 can promote the development of GC (Gao et al. 2017). However, the interaction between XN4 and NOX4 in ferroptosis remains unclear. Here, we measured the levels of ferroptosis-related proteins (GPX4 and PTGS2) and NOX4 during the induction of GC cell death by XN4. We found that NOX4 and PTGS2 expression was

upregulated and GPX expression was reduced following XN4 treatment. However, DFO and liproxstatin-1 abrogated the XN4-induced changes in ferroptosis-related proteins and NOX4 expression. NOX4 suppression has been shown previously to prevent the production of MDA (Wang et al. 2018), suggesting that it might be effective in mitigating ferroptosis-associated diseases. To further investigate whether NOX4 was implicated in XN4-induced ferroptosis, GC cells were treated with si-NOX4 and XN4. The MTT assay elucidated that the XN4-induced reduction in the viability of GC cells was counteracted by NOX4 knockdown. The LDH release assay also showed that depletion of NOX4 significantly reduced cell death, Fe^{2+} levels, and the MDA content of GC cells following XN4 treatment. Furthermore, silencing NOX4 resulted in a reduction in the XN4-induced changes in the levels of ferroptosis-related proteins, which shows the ability of NOX4 inhibitors to abolish ferroptosis, indicating the potential for developing combinational therapies. The collective results demonstrate that XN4 induced ferroptosis in GC cells by upregulating NOX4 expression.

This study has certain limitations. For instance, we used the GC cell lines SGC-7901 and BGC-823 to explore the possible role of XN4 in ferroptosis of GC cells, but metastatic GC is different. Therefore, further studies are needed to validate our results in additional cell lines, such as KATOIII or NCI-N87, as well as in tumour xenografts. Moreover, based on the results of this study, we can only propose that XN4 regulates NOX4 expression to mediate ferroptosis in GC cells; the detailed molecular mechanism by which XN4 regulates NOX4 requires further elucidation and will be one of the future directions of our research.

Conclusions

Our results suggest that the Nov derivative XN4 induced Fe^{2+} -dependent GC cell death, which differs from apoptosis, necrosis, or pyroptosis. XN4 facilitated Fe^{2+} accumulation in GC cells by upregulating TF and TFR, promoted mitochondrial damage and lipid peroxidation, increased hydrogen peroxide and ROS levels, and diminished GSH levels. Mechanistically, XN4 promotes ferroptosis in GC cells through upregulation of NOX4 expression. Thus, this study suggests that XN4 should be considered for use as a novel treatment strategy for GC, although further investigation is needed.

Author contributions

Conceived and designed the analysis: Liu Z; Li R. Collected the data: Li R; Yin B. Contributed data or analysis tools: Yin B; Zeng D. Performed the analysis: Li R; Yin B. Wrote the paper: Yin B. and Zeng D.

Disclosure statement

Conflict of interest relevant to this article was not reported.

Funding

Thanks for the support of the grant from the Changsha Municipal Natural Science Foundation (No. Kq1901078).

References

- Bray F, Ferlay J, Soerjomataram I, Siegel RL, Torre LA, Jemal A. 2018. Global cancer statistics 2018: globocan estimates of incidence and mortality worldwide for 36 cancers in 185 countries. *CA Cancer J Clin.* 68(6): 394–424.
- Cao JY, Dixon SJ. 2016. Mechanisms of ferroptosis. *Cell Mol Life Sci.* 73(11–12):2195–2209.
- Chen W, Zheng R, Baade PD, Zhang S, Zeng H, Bray F, Jemal A, Yu XQ, He J. 2016. Cancer statistics in China, 2015. *CA Cancer J Clin.* 66(2): 115–132.
- Dixon SJ, Lemberg KM, Lamprecht MR, Skouta R, Zaitsev EM, Gleason CE, Patel DN, Bauer AJ, Cantley AM, Yang WS, et al. 2012. Ferroptosis: an iron-dependent form of nonapoptotic cell death. *Cell.* 149(5):1060–1072.
- Dlugosz A, Janecka A. 2017. Novobiocin analogs as potential anticancer agents. *Mini Rev Med Chem.* 17(9):728–733.
- Fearnhead HO, Vandenabeele P, Vanden Berghe T. 2017. How do we fit ferroptosis in the family of regulated cell death? *Cell Death Differ.* 24(12): 1991–1998.
- Friedmann Angeli JP, Schneider M, Proneth B, Tyurina YY, Tyurin VA, Hammond VJ, Herbach N, Aichler M, Walch A, Eggenhofer E, et al. 2014. Inactivation of the ferroptosis regulator GPX4 triggers acute renal failure in mice. *Nat Cell Biol.* 16(12):1180–1191.
- Gao M, Monian P, Quadri N, Ramasamy R, Jiang X. 2015. Glutaminolysis and transferrin regulate ferroptosis. *Mol Cell.* 59(2):298–308.
- Gao X, Sun J, Huang C, Hu X, Jiang N, Lu C. 2017. Rnai-mediated silencing of NOX4 inhibited the invasion of gastric cancer cells through JAK2/STAT3 signaling. *Am J Transl Res.* 9:4440–4449.
- Hanahan D, Weinberg RA. 2011. Hallmarks of cancer: the next generation. *Cell.* 144(5):646–674.
- Hao S, Yu J, He W, Huang Q, Zhao Y, Liang B, Zhang S, Wen Z, Dong S, Rao J, et al. 2017. Cysteine dioxygenase 1 mediates erastin-induced ferroptosis in human gastric cancer cells. *Neoplasia.* 19(12):1022–1032.
- Hong SH, Lee DH, Lee YS, Jo MJ, Jeong YA, Kwon WT, Choudry HA, Bartlett DL, Lee YJ. 2017. Molecular crosstalk between ferroptosis and apoptosis: emerging role of er stress-induced p53-independent puma expression. *Oncotarget.* 8(70):115164–115178.
- Hou W, Xie Y, Song X, Sun X, Lotze MT, Zeh HJ 3rd, Kang R, Tang D. 2016. Autophagy promotes ferroptosis by degradation of ferritin. *Autophagy.* 12(8):1425–1428.
- Hu X, Xu Y, Xu H, Jin C, Zhang H, Su H, Li Y, Zhou K, Ni W. 2021. Progress in understanding ferroptosis and its targeting for therapeutic benefits in traumatic brain and spinal cord injuries. *Front Cell Dev Biol.* 9:705786.
- Jiang L, Kon N, Li T, Wang SJ, Su T, Hibshoosh H, Baer R, Gu W. 2015. Ferroptosis as a p53-mediated activity during tumour suppression. *Nature.* 520(7545):57–62.
- Le Bras G, Radanyi C, Peyrat JF, Brion JD, Alami M, Marsaud V, Stella B, Renoir JM. 2007. New novobiocin analogues as antiproliferative agents in breast cancer cells and potential inhibitors of heat shock protein 90. *J Med Chem.* 50(24):6189–6200.
- Lettni G, Maddalena F, Sisinni L, Condelli V, Matassa DS, Costi MP, Simoni D, Esposito F, Landriscina M. 2017. Trap1: a viable therapeutic target for future cancer treatments? *Expert Opin Ther Targets.* 21(8):805–815.
- Li J, Lan T, Zhang C, Zeng C, Hou J, Yang Z, Zhang M, Liu J, Liu B. 2015. Reciprocal activation between IL-6/STAT3 and NOX4/AKT signalings promotes proliferation and survival of non-small cell lung cancer cells. *Oncotarget.* 6(2):1031–1048.
- Linkermann A, Skouta R, Himmerkus N, Mulay SR, Dewitz C, De Zen F, Prokai A, Zuchtriegel G, Krombach F, Welz PS, et al. 2014. Synchronized renal tubular cell death involves ferroptosis. *Proc Natl Acad Sci USA.* 111(47):16836–16841.
- Ooki A, Yamaguchi K. 2021. The beginning of the era of precision medicine for gastric cancer with fibroblast growth factor receptor 2 aberration. *Gastric Cancer.* 24(6):1169–1183.
- Park MW, Cha H1W, Kim J, Kim JH, Yang H, Yoon S, Boonpraman N, Yi SS, Yoo ID, Moon JS. 2021. Nox4 promotes ferroptosis of astrocytes by oxidative stress-induced lipid peroxidation via the impairment of mitochondrial metabolism in Alzheimer's diseases. *Redox Biol.* 41:101947.
- Pavlova NN, Thompson CB. 2016. The emerging hallmarks of cancer metabolism. *Cell Metab.* 23(1):27–47.
- Shono T, Yokoyama N, Uesaka T, Kuroda J, Takeya R, Yamasaki T, Amano T, Mizoguchi M, Suzuki SO, Nihiro H, et al. 2008. Enhanced expression of NADPH oxidase NOX4 in human gliomas and its roles in cell proliferation and survival. *Int J Cancer.* 123(4):787–792.
- Skouta R, Dixon SJ, Wang J, Dunn DE, Orman M, Shimada K, Rosenberg PA, Lo DC, Weinberg JM, Linkermann A, et al. 2014. Ferrostatins inhibit

- oxidative lipid damage and cell death in diverse disease models. *J Am Chem Soc.* 136(12):4551–4556.
- Stockwell BR, Friedmann Angeli JP, Bayir H, Bush AI, Conrad M, Dixon SJ, Fulda S, Gascon S, Hatzios SK, Kagan VE, et al. 2017. Ferroptosis: a regulated cell death nexus linking metabolism, redox biology, and disease. *Cell.* 171(2):273–285.
- Sun X, Yang S, Feng X, Zheng Y, Zhou J, Wang H, Zhang Y, Sun H, He C. 2020. The modification of ferroptosis and abnormal lipometabolism through overexpression and knockdown of potential prognostic biomarker perilipin2 in gastric carcinoma. *Gastric Cancer.* 23(2):241–259.
- Tang CT, Lin XL, Wu S, Liang Q, Yang L, Gao YJ, Ge ZZ. 2018. NOX4-driven ROS formation regulates proliferation and apoptosis of gastric cancer cells through the gli1 pathway. *Cell Signal.* 46:52–63.
- Wagner AD, Syn NL, Moehler M, Grothe W, Yong WP, Tai BC, Ho J, Unverzagt S. 2017. Chemotherapy for advanced gastric cancer. *Cochrane Database Syst Rev.* 8:CD004064.
- Wang Z, Ding Y, Wang X, Lu S, Wang C, He C, Wang L, Piao M, Chi G, Luo Y, et al. 2018. Pseudolaric acid B triggers ferroptosis in glioma cells via activation of NOX4 and inhibition of XCT. *Cancer Lett.* 428:21–33.
- Wu L, Chen X, Huang L, Tian J, Ke F, Xu J, Chen Y, Zheng M. 2015. A novobiocin derivative, XN4, inhibits the proliferation of chronic myeloid leukemia cells by inducing oxidative DNA damage. *PLOS One.* 10(4): e0123314.
- Wu LX, Xu JH, Zhang KZ, Lin Q, Huang XW, Wen CX, Chen YZ. 2008. Disruption of the BCR-ABL/Hsp90 protein complex: a possible mechanism to inhibit BCR-ABL-positive human leukemic blasts by novobiocin. *Leukemia.* 22(7):1402–1409.
- Yang WS, SriRamaratnam R, Welsch ME, Shimada K, Skouta R, Viswanathan VS, Cheah JH, Clemons PA, Shamji AF, Clish CB, et al. 2014. Regulation of ferroptotic cancer cell death by GPX4. *Cell.* 156(1–2): 317–331.
- Zhang H, Deng T, Liu R, Ning T, Yang H, Liu D, Zhang Q, Lin D, Ge S, Bai M, et al. 2020. CAF secreted MIR-522 suppresses ferroptosis and promotes acquired chemo-resistance in gastric cancer. *Mol Cancer.* 19(1):43–59.
- Zhang H, Wang Z, Liu Z, Du K, Lu X. 2021. Protective effects of dexazoxane on rat ferroptosis in doxorubicin-induced cardiomyopathy through regulating HMBG1. *Front Cardiovasc Med.* 8:685434.
- Zhang Y, Shi J, Liu X, Feng L, Gong Z, Koppula P, Sirohi K, Li X, Wei Y, Lee H, et al. 2018. BAP1 links metabolic regulation of ferroptosis to tumour suppression. *Nat Cell Biol.* 20(10):1181–1192.
- Zhao H, Hu H, Chen B, Xu W, Zhao J, Huang C, Xing Y, Lv H, Nie C, Wang J, et al. 2021. Overview on the role of e-cadherin in gastric cancer: dysregulation and clinical implications. *Front Mol Biosci.* 8:689139.